remote sensing

MDPI

Article

Estimation of Chlorophyll-A Concentration with Remotely Sensed Data for the Nine Plateau Lakes in Yunnan Province

Dong Wang [1], Bo-Hui Tang [1,2,*], Zhitao Fu [1], Liang Huang [1], Menghua Li [1], Guokun Chen [1] and Xuejun Pan [3]

[1] Faculty of Land Resource Engineering, Kunming University of Science and Technology, Kunming 650093, China
[2] Institute of Geographic Sciences and Natural Resources Research, Chinese Academy of Sciences, Beijing 100101, China
[3] Faculty of Environmental Science and Engineering, Kunming University of Science and Technology, Kunming 650093, China
* Correspondence: tangbh@kust.edu.cn

Abstract: The quantitative retrieval of the chlorophyll-a concentration is an important remote sensing method that is used to monitor the nutritional status of water bodies. The high spatial resolution of the Sentinel-2 MSI and its subdivision in the red-edge band highlight the characteristics of water chlorophyll-a, which is an important detection tool for assessing water quality parameters in plateau lakes. In this study, the Nine Plateau Lakes in the Yunnan-Kweichow Plateau of China were selected as the study area. Using Sentinel-2 MSI transit images and in situ measured chlorophyll-a concentration as the data source, the chlorophyll-a concentrations of plateau lakes (CCAPLs) were investigated, and the surface temperatures of plateau lakes (STPLs) were retrieved to verify the hypothesis that the lake surface temperature could increase the chlorophyll-a concentration. By comparing feature importance using a random forest (RF), the Sentinel-2 MSI surface reflectance and in situ data were linearly fitted using four retrieval spectral indices with high feature importance, and the accuracy of the estimated concentration of chlorophyll-a was evaluated by monitoring station data in the same period. Then, Landsat-8 TIRS Band 10 data were used to retrieve the STPL with a single-channel temperature retrieval algorithm and to verify the correlation between the STPL and the CCAPL. The results showed that the retrievals of the CCAPL and the STPL were consistent with the actual situation. The root-mean-square error (RMSE) of the fifteenth normalized difference chlorophyll-a index (NDCI15) was 0.0249. When the CCAPL was greater than 0.05 mg/L and the STPL was within 28–34 °C, there was a positive linear correlation between the CCAPL and the STPL. These results will provide support for the remote sensing monitoring of eutrophication in plateau lakes and will contribute to the scientific and effective management of plateau lakes.

Keywords: chlorophyll-a; Landsat-8; plateau lakes; Sentinel-2; surface temperature

Citation: Wang, D.; Tang, B.-H.; Fu, Z.; Huang, L.; Li, M.; Chen, G.; Pan, X. Estimation of Chlorophyll-A Concentration with Remotely Sensed Data for the Nine Plateau Lakes in Yunnan Province. *Remote Sens.* **2022**, *14*, 4950. https://doi.org/10.3390/rs14194950

Academic Editors: Jiayi Pan, Hongsheng Zhang, Bo Huang and Adam T. Devlin

Received: 6 September 2022
Accepted: 30 September 2022
Published: 4 October 2022

1. Introduction

In recent years, the water quality of plateau lakes has been a topic of concern for the government and the public. Chlorophyll-a is an important indicator that reflects the nutritional status of plateau water and is used to monitor the outbreak of cyanobacteria blooms. Monitoring the chlorophyll-a concentration can help to prevent further deterioration of the water quality [1]. Traditional chlorophyll-a-concentration-monitoring methods are inconvenient, complicated and time-consuming [2]. Using an in-depth study of water spectral characteristics and the improvement of chlorophyll-a retrieval model, remote sensing images can more accurately simulate chlorophyll-a content, combined with the hydrological parameters, geographical location, natural resources and other information, water pollution and water quality change trends can be found effectively [3–5]. In the early stage, the retrieval of chlorophyll-a concentration using remote sensing was mainly carried

out around a class of water bodies, such as the ocean, and was generally based on the ratio of blue and green bands, which achieved good results. However, the application of such algorithms in plateau lakes with complex optical properties is limited [6,7]. An updated chlorophyll-a retrieval model for plateau lakes needs to account for the differences in the water, the significant influence of humans, the distinct regional characteristics, the components of water being extremely complex, the difficulty of the retrieval of the chlorophyll-a concentration and the poor portability of the retrieval model [8,9]. In addition, due to the uneven distribution of plateau lakes, the spatial resolution of satellite data is required to be high, and the amount of available data is lower; therefore, the retrieval of the chlorophyll-a concentration of plateau lakes (CCAPL) has always been the focus and difficulty in the research [10–12]. Although researchers have recently developed a "reflection peak", a "band algorithm", an "index algorithm" and "machine learning", as well as a series of calculation methods to determine the chlorophyll-a concentration, this mainly involves the chlorophyll-a fluorescence peak and other sensitive bands of near-infrared and red bands, but it cannot achieve high precision and strong universality in plateau lakes [13–15]. The random forest (RF) algorithm can reduce the error and reflect the feature importance using the Gini coefficient [16]. It is now applied in the field of water quality remote sensing [17,18]. Based on plateau lakes and the inherent optical properties of chlorophyll-a, band combinations were established. The Gini coefficient is used to calculate the feature importance in RF, which is good at selecting the optimal retrieval model and achieves the high-precision retrieval of the CCAPL.

Studies showed that within a certain temperature range, the lake surface temperature contributes to the growth of algae, and there is often a positive correlation between the STPL and the distribution of the CCAPL, but this has not been verified in many lakes.

In this study, the Sentinel-2 MSI surface reflectance data and in situ data were used to compare the importance of different bands and band combinations according to the feature importance of the RF algorithm. The retrieval model of CCAPL was selected and the accuracy of retrieval results was evaluated. Based on the single-channel algorithm, the STPL was retrieved using the Landsat-8 TIRS data, and the correlation between the STPL and the CCAPL distribution was verified. Section 2 presents the study area and data, including the satellite data and ground observation site data. The retrieval theory of the CCAPL and STPL is introduced in Section 3. Section 4 presents the retrieval results of the CCAPL and STPL and their correlation analysis. In the fifth section, the shortcomings of the experiment are discussed, and the future development trend is discussed. The sixth part summarizes the selection of the chlorophyll-a retrieval model, the retrieval results of chlorophyll-a concentration in nine plateau lakes, and the correlation between the lake surface temperature and the chlorophyll-a concentration.

2. Materials

2.1. Study Area

The Yunnan-Kweichow plateau lakes area is one of China's Five Great Lakes and shows significant lake type diversity, including nine plateau lakes in Yunnan province; Dianchi Lake (DCL), Erhai Lake (EHL), Fuxian Lake (FXL), Chenghai Lake (CHL), Lugu Lake (LGL), Qilu Lake (LYL), Xingyun Lake (XYL), Yangzong Lake (YZL) and Yilong Lake (YLL) are the main lakes in the Yunnan-Kweichow plateau lakes and are referred to as the "Nine Plateau Lakes". They are concentrated in the northwest and central Yunnan province at an average elevation of over 1800 m. The unique geological features of Yunnan province led to the creation of nine plateau lakes, of which Fuxian Lake is the deepest with a depth of 155 m. Dianchi Lake is the largest, covering 306.3 square kilometers of water. In recent years, with the rapid development of the economy and society, the lakes' ecological environment deserves more attention. According to the evaluation standard of lake eutrophication in China, when the comprehensive trophic level index (TLI) calculated using chlorophyll-a is above 50, the lake is in a eutrophic state, where 50–60 denotes mild eutrophication, 60–70 denotes moderate eutrophication, and a TLI greater than 70 denotes severe eutrophication.

According to the official statistics released by the Yunnan Department of Ecology and Environment in January 2022, Qilu Lake and Yilong Lake are in a severe eutrophic state; Xingyun Lake is in a moderate eutrophic state; and Dianchi Lake, Erhai Lake, Yangzong Lake and Chenghai Lake are in a mild eutrophic state. In this study, the Nine Plateau Lakes were selected as the study areas. The lake locations are shown in Figure 1. The monitoring stations of Dianchi Lake are also shown in this figure.

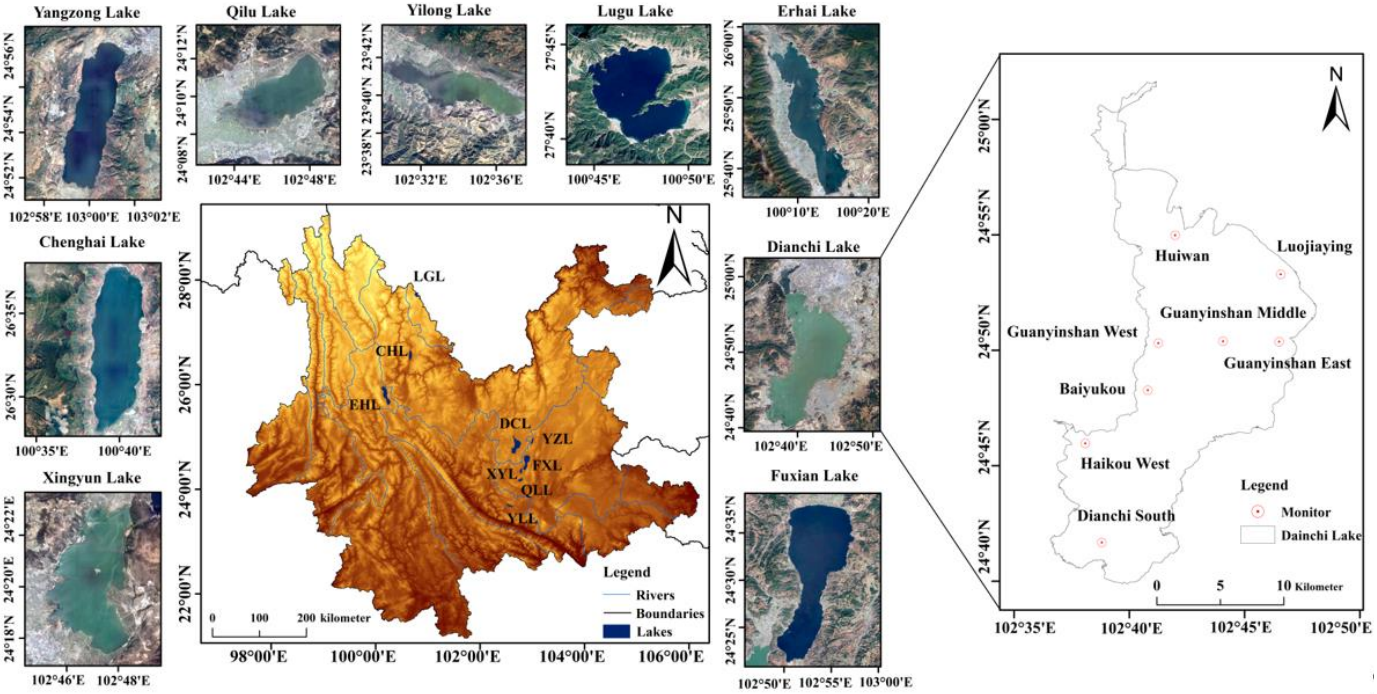

Figure 1. Satellite images of Nine Plateau Lakes, their geographical locations, and the monitoring station of Dianchi Lake.

2.2. Data

Landsat-8, the eighth satellite launched by the National Aeronautics and Space Administration (NASA) for the land observation program, carries a thermal infrared sensor (TIRS) with a resolution of 100 m, providing two thermal infrared channels, which can observe and record the thermal radiation of the target well. Since the operation of the TIRS sensor began, many temperature retrieval algorithms for TIRS Band 10 and Band 11 have been formed, and good results have been achieved [19]. However, due to the large calibration deviation of Band 11, Band 10 is often used for surface temperature retrieval [20]. Based on the platform provided by the United States Geological Survey (USGS), this study downloaded the image of the thermal infrared channel on 9 August 2020 of the Nine Plateau Lakes, and the cloud cover of the remote sensing images was controlled to less than 10%. The band information is shown in the following Table 1.

The multispectral imager (MSI) carried by Sentinel-2 is 786 km high, can cover 13 wavebands with an image width of 290 km and has a revisit period of 10 days. The Sentinel-2 satellite data is the only one with three bands in the red-edge range, which is very effective for monitoring the CCAPL. For domestic users, the ESA released the atmospheric apparent reflectance product (a Level-1C data product) after ortho-rectification and sub-pixel geometric precision correction, and also released the definition of Level-2A data by Sen2cor, which is a plug-in specialized in producing Level-2A data. Level-2A data is surface reflectivity data, but this Level-2A data needs to be produced by users as required. The Google Earth Engine (GEE) platform provides Level-2A data products. Based on the GEE platform, the MSI Sentinel-2 Level-2A remote sensing reflectance data from August 2020 were used in this study. The satellite parameters are shown in Table 2.

Table 1. Landsat-8 band parameters.

Bands	Name	Wavelength (nm)	Resolution (m)
Band 1	Coastal	0.433–0.453	30
Band 2	Blue	0.450–0.515	30
Band 3	Green	0.525–0.600	30
Band 4	Red	0.630–0.680	30
Band 5	NIR	0.845–0.885	30
Band 6	SWIR 1	1.560–1.660	30
Band 7	SWIR 2	2.100–2.300	30
Band 8	Pan	0.500–0.680	15
Band 9	Cirrus	1.360–1.390	30
Band 10	TIRS 1	10.60–11.19	100
Band 11	TIRS 2	11.50–12.51	100

Table 2. Sentinel-2 band parameters.

Bands	Name	Wavelength (nm)	Resolution (m)
Band 1	Coastal aerosol	0.433–0.453	60
Band 2	Blue	0.458–0.523	10
Band 3	Green	0.543–0.578	10
Band 4	Red	0.650–0.680	10
Band 5	Vegetation red edge 1	0.698–0.713	20
Band 6	Vegetation red edge 2	0.733–0.748	20
Band 7	Vegetation red edge 3	0.773–0.793	20
Band 8	NIR	0.785–0.900	10
Band 8A	Vegetation red edge 4	0.935–0.955	20
Band 9	Water vapor	1.360–1.390	60
Band 11	SWIR 1	1.565–1.655	20
Band 12	SWIR 2	2.100–2.280	20

Due to the special geographical location and uneven distribution of the plateau lakes, it is difficult to obtain the measured chlorophyll-a concentration data on the surface of the plateau lakes. In this study, the in situ measured chlorophyll-a concentrations in 2020 of the Nine Plateau Lakes in the Yunnan-Kweichow Plateau of China was published by Yunnan Provincial Department of Ecology and Environment and Nanjing Institute of Geography and Limnology, Chinese Academy of Sciences. The chlorophyll-a concentration was measured in the laboratory using the ethanol spectrophotometer method [21]. The in situ measurements of the chlorophyll-a concentration in some lakes were missing or the amount of available data was lower. After the measured data were obtained, the mean value and standard deviation of the data were calculated, and we considered the points that were three standard deviations from the mean to be outliers and were removed. The monitoring time and quantity of chlorophyll-a concentration obtained are shown in Table 3.

Table 3. Sampling time and the number of chlorophyll-a sampling points.

Name	Monitoring Time	* Number of Sampling Points
Dianchi Lake	20200623	40
Fuxian Lake	20200622	30
Chenghai Lake	20200701	19
Erhai Lake	20200625	17
Lugu Lake	20200618	25
Qilu Lake	20200629	14
Xingyun Lake	20200627	17
Yangzong Lake	20200712	16
Yilong Lake	20200625	15

* The chlorophyll-a in situ measured unit is mg/L.

3. Methods

3.1. Water Body Extraction

At present, the commonly used methods for water body extraction include the normalized difference water index (NDWI) and improved normalized difference water index (MNDWI). The traditional normalized difference water index (NDWI) [22] is mainly calculated using the green band and red band. Since water has strong absorption in the near-infrared band and vegetation has strong reflectivity in the near-infrared band, it is usually used to differentiate between the waterbody and shore vegetation. Although the NDWI can suppress vegetation information to a large extent, the extracted water is often confused with surrounding buildings and soil, resulting in an excessive extracted waterbody area, and thus, it cannot achieve a good water extraction effect. In this study, an improved normalized difference water index (MNDWI) was used for water extraction based on the GEE platform [23]. The MNDWI is based on the shortwave infrared band instead of the near-infrared band, which effectively suppresses building and soil information and greatly reduces background noise, and the index significantly improves measurements of the characteristics of The Nine Plateau Lakes water area. The efficiency of water body extraction is greatly improved. The equation can be expressed as follows:

$$\mathrm{MNDWI} = \frac{\rho_{(\mathrm{Green})} - \rho_{(\mathrm{SWIR1})}}{\rho_{(\mathrm{Green})} + \rho_{(\mathrm{SWIR1})}} \quad (1)$$

where MNDWI represents the improved normalized difference water index, $\rho_{(\mathrm{Green})}$ represents the green band reflectance and $\rho_{(\mathrm{SWIR1})}$ represents the shortwave infrared band reflectance; an MNDWI value greater than 0 signifies an area of water.

3.2. Retrieval Model Construction of the CCAPL

Chlorophyll-a in lakes has obvious bio-optic properties, and thus, many spectral indices related to the chlorophyll-a concentration were proposed based on specific assumptions, and the chlorophyll-a concentration retrieval is realized by establishing statistical relations [24]. As can be seen from the previous spectral characteristics of plateau lakes, the absorption characteristics of chlorophyll-a are obviously different in the band of 400~730 nm, and the reflection spectrum has obvious characteristics of wave peaks and troughs. When the wave band is near 400–500 nm, the water reflectance is generally low due to the strong absorption of blue light by chlorophyll-a [25]. At 500~620 nm, due to the weak absorption of chlorophyll-a and carotin in water and the scattering effect of suspended particles, the reflectance of water produces a wave peak, whose peak height can be used to measure the chlorophyll-a concentration. At 620~670 nm, the strong absorption of red by chlorophyll-a leads to a distinct trough [26]. In the vicinity of 670~730 nm, there is another obvious reflection peak, often called the "fluorescence peak", which is the key to determining the chlorophyll-a concentration because the absorption coefficient of water and chlorophyll-a reaches the minimum here [27]. According to the inherent optical properties of chlorophyll-a in plateau lakes, relevant literature of chlorophyll-a concentration retrieval in recent years was consulted, and a spectral index of chlorophyll-a retrieval was established based on an empirical model and a semi-analytical model.

The selected wavelengths focus on the reflection peak or absorption valley of the chlorophyll-a reflection spectrum to construct a single band index:

$$C_{chl\text{-}a} = A + B \cdot \rho_i \quad (2)$$

where $C_{Chl\text{-}a}$ represents the CCAPL, A and B are the correlation coefficients of the regression model, and ρ_i (i = B2, B3, B4, B5, B6, B7, B8, B8A) is the water reflectance of a band selected by the Sentinel-2 data sources.

The ratio index was constructed by selecting two bands with obvious reflection spectrum characteristics of chlorophyll-a to enlarge the difference between the absorption valley and reflection peak of chlorophyll-a:

$$C_{chl\text{-}a} = C + D \cdot \frac{\rho_i}{\rho_j} \tag{3}$$

where $C_{Chl\text{-}a}$ represents the CCAPL, C and D are the correlation coefficients of the regression model, and ρ_i and ρ_j (i, j = B2, B3, B4, B5, B6, B7, B8, B8A) are the water reflectances of two bands selected by the Sentinel-2 data sources.

Two bands with obvious spectral characteristics of chlorophyll-a reflection were selected to construct the normalized chlorophyll-a index, and the comparison of the reflectance of the two bands was further enhanced using nonlinear stretching:

$$C_{chl\text{-}a} = E + F \cdot \frac{\rho_i - \rho_j}{\rho_i + \rho_j} \tag{4}$$

where $C_{Chl\text{-}a}$ represents the CCAPL, E and F are the correlation coefficients of the regression model, and ρ_i and ρ_j (i, j = B2, B3, B4, B5, B6, B7, B8, B8A) are the water reflectances of the two bands selected by the Sentinel-2 data sources.

Three characteristic bands were selected and combined with mathematical derivation and statistical theory to construct the three-band index:

$$C_{chl\text{-}a} = G + H \cdot ({\rho_i}^{-1} - {\rho_j}^{-1}) \cdot \rho_k \tag{5}$$

where $C_{Chl\text{-}a}$ represents the CCAPL; G and H are the correlation coefficients of the regression model; and ρ_i, ρ_j and ρ_k (i, j, k = B2, B3, B4, B5, B6, B7, B8, B8A) are the water reflectances of the three bands selected by the Sentinel-2 data sources.

3.3. RF Algorithm Feature Selection

The RF algorithm has excellent anti-noise ability, which makes it useful in various fields [28,29]. The feature importance in the RF algorithm can distinguish the importance of various bands or a combination thereof. The larger the feature importance is, the more important the bands are, i.e., the more correlated the bands or combinations are with chlorophyll-a. The feature importance of RF is calculated as follows [30].

We used the variable importance measure (*VIM)* to represent the feature importance. *GI* represents the Gini coefficient. Assuming m features X_1, X_2, … , X_C, the Gini index score $VIM_j^{(Gini)}$ is calculated for each feature X_j, where the Gini coefficient GI_m is expressed as follows:

$$GI_m = 1 - \sum_{k=1}^{|K|} p^2 mk \tag{6}$$

where the Gini coefficient represents the probability that a randomly selected sample in the sample set will be misclassified, K is the number of categories and pmk represents the proportion of category k in node m.

The feature importance Xj on node m, that is, the change in Gini coefficient before and after node m is

$$VIM_{jm}{}^{(Gini)} = GI_m - GI_l - GI_r \tag{7}$$

where GI_l and GI_r represent the Gini coefficients of the left and right nodes, respectively.

Assuming that M is the set of nodes that appear in decision tree i, then the importance of Xj in the ith tree is

$$VIM_{ij}{}^{(Gini)} = \sum_{m \in M} VIM_{jm}{}^{(Gini)} \tag{8}$$

When the number of decision trees is n, the feature importance is

$$VIM_j^{(Gini)} = \sum_{i=1}^{n} VIM_{ij}^{(Gini)} \quad (9)$$

In this study, the RF algorithm was constructed based on the GEE platform. The constructed spectral index was input as the feature and sorted by the feature importance. The larger the feature importance was, the higher the correlation with chlorophyll-a; the spectral index with the highest correlation was selected as the spectral index of the chlorophyll-a concentration retrieval.

3.4. CCAPL Retrieval and Evaluation Methods

First, several spectral indices with large feature importance were selected as the retrieval models of chlorophyll-a concentration, and the chlorophyll-a concentration was retrieved through linear fitting based on the Sentinel-2 MSI surface reflectance data and in situ measured chlorophyll-a concentration data. Second, the root-mean-square error (RMSE), mean absolute error (MAE) and mean absolute percentage error (MAPE) were used to evaluate the accuracy of the CCAPL retrieval results.

The RMSE is the square root of the ratio of the square sum of the deviation between the observed value and the truth value for n observations, which can represent the degree of dispersion of data well. A small value of RMSE indicates a high accuracy. The equation can be expressed as follows:

$$\mathrm{RMSE} = \sqrt{\frac{1}{n}\sum_{i=1}^{n}(Y_i - X_i)^2} \quad (10)$$

where RMSE represents the root-mean-square error, n represents the number of observed values, and X_i and Y_i represent the retrieval value and true value of the CCAPL, respectively.

The MAE is the average of the absolute error between the observed value and the real value. The smaller the MAE value is, the closer the retrieval value is to the real value. The equation can be expressed as follows:

$$\mathrm{MAE} = \frac{1}{n}\sum_{i=1}^{n}|Y_i - X_i| \quad (11)$$

where MAE represents the mean absolute error; n represents the number of observed values; and X_i and Y_i represent the retrieval value and true value of the CCAPL, respectively.

The MAPE is the average absolute percentage error, where a MAPE value of 0% means a perfect model and a MAPE greater than 100% means an inferior model. The equation can be expressed as follows:

$$\mathrm{MAPE} = \frac{1}{n}\sum_{i=1}^{n}\left|\frac{Y_i - X_i}{Y_i}\right| \times 100\% \quad (12)$$

where MAPE represents the mean absolute percentage error; n represents the number of observed values; and X_i and Y_i represent the retrieval value and true value of the CCAPL, respectively.

3.5. Lake Surface Temperature Retrieval

The water surface temperature generally refers to the average surface temperature at a depth of more than 10 cm or the average temperature of a thick water layer at 1 m. Because water has a strong absorption effect in the thermal infrared band, the temperature of the water surface measured by remote sensing is actually the thermal radiation brightness of the top layer of water, which is called the "skin temperature" [31]. According to the radiative transfer equation, the real lake temperature (physical temperature) of water can

be obtained only after considering the specific emissivity of water. However, given that the specific emissivity of water is 0.995 in actual observations, which is very close to that of a black body, the temperature of a water body is often expressed using the measured brightness temperature.

The basis for retrieving the lake surface temperature using remote sensing data is the heat radiative transfer equation constituted by the quantization of Planck's Law [32]. According to the sensor settings, it can be divided into a single-band method, double-band method (split window algorithm) and multi-band method. The Landsat-8 TIRS sensor has two thermal infrared bands, namely, Band 10 and Band 11, and thus, it can retrieve the surface temperature through dual bands and a single band. Because the TIRS Band 10 has a lower atmospheric absorption region and a more accurate atmospheric transmittance, Band 10 is adopted for temperature retrieval.

The basic principle of retrieving the temperature based on a radiative transfer model is as follows: first, estimate the influence of the atmosphere on the surface thermal radiation, then subtract the atmospheric influence to obtain the surface thermal radiation intensity, and finally convert the thermal radiation intensity into the surface temperature. The radiation brightness observed by the satellite sensor consists of three parts. The first part is the energy of the surface radiation reaching the satellite sensor through the atmosphere. The second part is the amount of energy that is radiated upward by the atmosphere, and the third part is the amount of energy that is radiated downward and reflected from the Earth's surface. The equation can be expressed as follows:

$$L_{TOA} = (\varepsilon \cdot B(T_S) + (1 - \varepsilon) \cdot L^{\downarrow}) \cdot \tau + L^{\uparrow} \tag{13}$$

Blackbody radiation is obtained via transposition:

$$B(T_S) = \left[L_{TOA} - L^{\uparrow} - \tau \cdot (1 - \varepsilon) \cdot L^{\downarrow}\right] / \tau \cdot \varepsilon \tag{14}$$

where L_{TOA} represents the radiation brightness, ε represents the surface-specific emissivity, T_S represents the real surface temperature, $B(T_S)$ represents the blackbody radiance, $L^{\downarrow}$ represents the downward atmospheric radiation, $L^{\uparrow}$ represents the upward atmospheric radiation and τ represents the atmospheric transmittance in the thermal infrared band.

The radiation brightness value is determined via radiation calibration. The calculation of the land surface emissivity is based on classifications. Vegetation coverage is first calculated (PV) using the mixed pixel decomposition method, and the land surface is roughly divided into water bodies, buildings and vegetation. According to the method proposed by Qin and Duan [33,34], the emissivities of a water body, vegetation and a building are 0.995, 0.982 and 0.967, respectively.

The equation of the water-specific emissivity and vegetation coverage can be expressed as follows:

$$\varepsilon = 0.004 P_V + 0.995 \tag{15}$$

$$P_V = (NDVI - NDVIS)/(NDVIV - NDVIS) \tag{16}$$

where ε represents the land surface emissivity, P_V represents the vegetation coverage, *NDVI* is the normalized vegetation index, *NDVIS* is the *NDVI* value of the area without vegetation coverage and *NDVIV* represents the *NDVI* value of a pixel completely covered by vegetation. The classification of vegetation coverage is based on an empirical coefficient, and an *NDVI* below 0.03 is regarded as pure bare soil, while an *NDVI* above 0.35 is regarded as pure vegetation.

Due to the different atmospheric parameters at different altitudes, the atmospheric radiation brightness is also different. In the study of the radiative transfer equation algorithm, the most important parameters are the values of the atmospheric upward radiation, atmospheric downward radiation and atmospheric transmittance. At present, the Atmospheric Correction Parameter Calculator (ACPC) can be used to simulate the process of

radiative transfer from the surface to the atmosphere to calculate the atmospheric upward radiation, atmospheric downward radiation and atmospheric transmittance.

The surface temperature can be calculated when the surface emissivity is known. The surface temperature of T_S in the formula can be obtained through the Planck function formula, which is as follows:

$$T_S = k_2 / \ln\left(\frac{k_1}{B(T_S)} + 1\right) \tag{17}$$

where T_S is the surface temperature, $B(Ts)$ is the blackbody radiation brightness, and k_1 and k_2 are the calibration constants of the Landsat-8 TIRS sensor (k_1 = 774.89, k_2 = 1321.08).

4. Results

4.1. Extraction Results of Water Bodies

The improved normalized differential water index was used to extract the water boundary. When the threshold value was greater than 0, the water boundary was extracted; the obtained results are shown in Figure 2, where the orange parts represent water bodies.

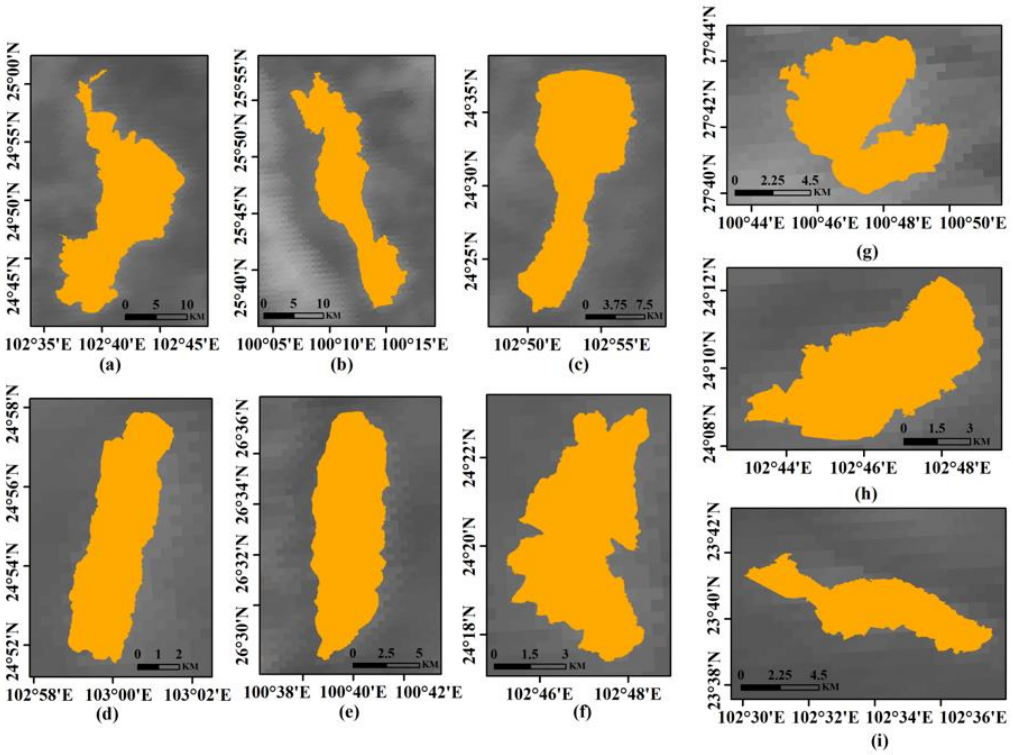

Figure 2. Nine plateau lake boundaries: (**a**) DCL, (**b**) ERL, (**c**) FXL, (**d**) YZL, (**e**) CHL, (**f**) XYL, (**g**) LGL, (**h**) QLL and (**i**) YLL.

4.2. CCAPL Model and Accuracy Evaluation

The RF algorithm was constructed in the GEE platform, and the in situ measured chlorophyll-a concentration was taken as the sample point. Based on the spectral analysis in Section 3.2, the reflection characteristics of plateau lakes are mainly located in the visible-to-near-infrared band, and thus, the multispectral band and the red-edge band of Sentinel-2 were selected for the chlorophyll-a concentration retrieval in this study. The single band, the band ratio, the normalized ratio index and the three-band index were calculated using Equations (2), (3), (4) and (5), respectively. The index models were used as the features of the random forest decision tree model. The results obtained from the calculation of the feature importance are shown in Table 4. The higher the feature importance, the stronger the correlation with the CCAPL.

Table 4. Feature importance computational results.

ID	Band	Index Model	Feature Importance
1	B2	B2	44.3066
2	B3	B3	43.9564
3	B4	B4	42.2547
4	B5	B5	43.6587
5	B6	B6	46.0333
6	B7	B7	45.0136
7	B8	B8	43.8657
8	B8A	B8A	39.3531
9	B8/B4	Divd1	35.9668
10	B8/B5	Divd2	37.7500
11	B8/B6	Divd3	46.0961
12	B8/B7	Divd4	38.5882
13	B8/B8A	Divd5	47.3490
14	B8A/B4	Divd6	36.2064
15	B8A/B5	Divd7	40.1768
16	B8A/B6	Divd8	44.6549
17	B8A/B7	Divd9	41.3910
18	B7/B4	Divd10	38.5530
19	B7/B5	Divd11	44.2034
20	B7/B6	Divd12	45.7065
21	B6/B5	Divd13	49.2723
22	B6/B4	Divd14	44.8093
23	B5/B4	Divd15	49.4467
24	B8 − B4/B8 + B4	NDCI1	37.6184
25	B8 − B5/B8 + B5	NDCI2	44.9984
26	B8 − B6/B8 + B6	NDCI3	46.9481
27	B8 − B7/B8 + B7	NDCI4	39.0772
28	B8 − B8A/B8 + B8A	NDCI5	46.5039
29	B8A − B4/B8A + B4	NDCI6	42.8151
30	B8A − B5/B8A + B5	NDCI7	43.4148
31	B8A − B6/B8A + B6	NDCI8	45.4098
32	B8A − B7/B8A + B7	NDCI9	48.7971
33	B7 − B4/B7 + B4	NDCI10	40.1548
34	B7 − B5/B7 + B5	NDCI11	40.1852
35	B7 − B6/B7 + B6	NDCI12	44.5754
36	B6 − B5/B6 + B5	NDCI13	41.0464
37	B6 − B4/B6 + B4	NDCI14	43.2968
38	B5 − B4/B5 + B4	NDCI15	56.2430
39	(1/B4 − 1/B5)·B6	TBI1	54.1088
40	(1/B4 − 1/B5)·B7	TBI2	44.7620
41	(1/B4 − 1/B5)·B8	TBI3	55.2735
42	(1/B4 − 1/B5)·B8A	TBI4	42.9489

Based on the reflection characteristics of the plateau lakes, the index models selected in this study were correlated with chlorophyll-a, and thus, the result of the feature importance of the difference was small. On this basis, four band combinations were selected for comparison, which could select the optimal chlorophyll-a retrieval model well. According to Table 4, the fifteenth normalized difference chlorophyll-a index (NDCI15), the first band index (TBI1), the third band index (TBI3) and the fifteenth divide index (Divd15) had the highest feature importance; therefore, they were selected as the spectral indexes of the CCAPL retrieval. The Sentinel-2 data and the in situ measured chlorophyll-a concentration data on the ground were used for the linear fitting of the CCAPL through four spectral indexes, and the fitting results are shown in Table 5.

As can be seen from Table 5, all four spectral indexes showed good retrieval effects for different plateau lakes. The R-squared value of Yangzong Lake with the NDCI15 model was the highest (0.8155), and that of Qilu Lake with the TBI3 model was the lowest (0.2313). The

linear fitting results of the four models of the Dianchi Lake area are shown in Figure 3. The CCAPL was predicted using four spectral index models, and the accuracy of the retrieval results was evaluated using the relative error, RMSE, MAE, MAPE and other accuracy verification indexes based on the data of 31 monitoring sites published by the Ministry of Ecology and Environment, as shown in Tables 6 and 7.

The NDCI15\TBI3\TBI1\Divd15 model had a good effect on the retrieval of the CCAPL through the error analysis and precision statistics results. Among them, NDCI15's RMSE, MAE and MAPE were 0.0249, 0.0142 and 26.30%, respectively. Compared with the three other spectral indexes, the NDCI15 model had the advantage of higher accuracy. This was because NDCI15 further improved the reflectance ratio of the two bands via the nonlinear stretching of Band 5 and Band 4, and had good stability and robustness to the difference between the spectral characteristics of the lakes in the plateau area.

Table 5. Linear fitting results.

Name	Model	Linear Fitting	R-Squared
Dianchi Lake	NDCI15	y = 0.0347 + 0.2832x	0.7246
	Divd15	y = −0.0408 + 0.0873x	0.7467
	TBI1	y = 0.0466 + 0.1435x	0.7298
	TBI3	y = 0.0453 + 0.1715x	0.7164
Erhai Lake	NDCI15	y = 0.0056 + 0.2084x	0.7631
	Divd15	y = −0.0944 + 0.1001x	0.7584
	TBI1	y = 0.0055 + 0.1204x	0.7539
	TBI3	y = 0.0056 + 0.1317x	0.7391
Fuxian Lake	NDCI15	y = 0.0019 + 0.0485x	0.7626
	Divd15	y = −0.0211 + 0.023x	0.766
	TBI1	y = 0.0019 + 0.0232x	0.7534
	TBI3	y = 0.0019 + 0.0257x	0.7504
Chenghai Lake	NDCI15	y = 0.0108 + 0.0367x	0.663
	Divd15	y = −0.0077 + 0.0184x	0.6614
	TBI1	y = 0.0107 + 0.0328x	0.6143
	TBI3	y = 0.0106 + 0.041x	0.6097
Lugu Lake	NDCI15	y = 0.0012 + 0.0058x	0.7093
	Divd15	y = −0.0004 + 0.0018x	0.6186
	TBI1	y = 0.0012 + 0.0039x	0.5177
	TBI3	y = 0.0014 + 0.0037x	0.2363
Qilu Lake	NDCI15	y = −0.0231 + 0.8493x	0.6342
	Divd15	y = −0.242 + 0.2593x	0.6349
	TBI1	y = 0.0488 + 0.2932x	0.3412
	TBI3	y = 0.0499 + 0.3327x	0.2313
Xingyun Lake	NDCI15	y = 0.0708 + 0.2692x	0.5455
	Divd15	y = −0.0071 + 0.0871x	0.5398
	TBI1	y = 0.0757 + 0.15x	0.5748
	TBI3	y = 0.0754 + 0.1734x	0.5476
Yangzong Lake	NDCI15	y = 0.0087 + 0.1689x	0.8155
	Divd15	y = −0.067 + 0.0759x	0.7878
	TBI1	y = 0.0091 + 0.0725x	0.7439
	TBI3	y = 0.0092 + 0.0718x	0.7257
Yilong Lake	NDCI15	y = 0.1193 + 0.6661x	0.6822
	Divd15	y = −0.0855 + 0.2255x	0.6861
	TBI1	y = 0.1285 + 0.4169x	0.6528
	TBI3	y = 0.0996 + 0.6013x	0.4051

Table 6. Relative error of the CCAPL retrieval model.

Lakes	Monitor Name	In Situ Value (mg/L)	Retrieved Value (mg/L)				Relative Error			
			Divd15	NDCI15	TBI1	TBI3	Divd15	NDCI15	TBI1	TBI3
Dianchi Lake	Huiwan	0.0752	0.1010	0.0992	0.0945	0.0931	34.29%	31.90%	25.70%	23.86%
	Luojiaying	0.0632	0.0946	0.0945	0.0965	0.0969	49.61%	49.57%	52.63%	53.34%
	Guanyinshan West	0.0594	0.0758	0.0753	0.0767	0.0765	27.54%	26.84%	29.09%	28.82%
	Guanyinshan Middle	0.0525	0.0902	0.0914	0.0889	0.0904	71.86%	74.13%	69.36%	72.23%
	Guanyinshan East	0.0670	0.1074	0.1044	0.1101	0.1080	60.29%	55.82%	64.40%	61.22%
	Baiyukou	0.0643	0.0886	0.0889	0.0882	0.0882	37.72%	38.21%	37.23%	37.25%
	Haikou West	0.0511	0.0638	0.0601	0.0671	0.0675	24.83%	17.63%	31.29%	32.03%
	Dianchi South	0.0582	0.0744	0.0737	0.0743	0.0739	27.87%	26.63%	27.67%	26.94%
Erhai Lake	Lake Center 1	0.0072	0.0063	0.0062	0.0061	0.0062	12.14%	13.21%	14.62%	14.06%
	Shuanglang	0.0095	0.0134	0.0133	0.0123	0.0118	41.05%	40.19%	29.67%	23.99%
	Xizhou	0.0093	0.0098	0.0098	0.0090	0.0088	5.52%	5.33%	2.71%	5.71%
	Lkae Center 2	0.0081	0.0119	0.0119	0.0115	0.0114	46.87%	46.38%	41.76%	40.90%
	Longkan	0.0079	0.0096	0.0096	0.0086	0.0084	21.65%	21.42%	9.01%	6.63%
	Lake Center 3	0.0068	0.0057	0.0056	0.0055	0.0056	16.18%	17.65%	19.12%	17.65%
Fuxian Lake	Xinhekou	0.0038	0.0034	0.0035	0.0034	0.0035	9.47%	8.66%	10.77%	8.32%
	Luchong	0.0044	0.0035	0.0035	0.0034	0.0035	20.74%	20.10%	21.84%	21.16%
	Haikou	0.0032	0.0026	0.0026	0.0026	0.0026	19.33%	18.56%	19.52%	19.96%
	Gushing	0.0037	0.0029	0.0029	0.0029	0.0029	21.90%	21.04%	22.04%	20.51%
Chenghai Lake	Lake Center	0.0094	0.0112	0.0113	0.0112	0.0111	19.12%	20.10%	19.19%	18.16%
	Banhaizi	0.0088	0.0104	0.0105	0.0104	0.0103	17.77%	18.88%	18.37%	17.28%
	Dongyanzi	0.0076	0.0095	0.0096	0.0097	0.0094	25.42%	26.27%	27.48%	23.99%
Lugu Lake	Lake Center North	0.0015	0.0017	0.0016	0.0018	0.0019	12.20%	8.18%	19.79%	26.40%
	Lake Center South	0.0018	0.0022	0.0022	0.0030	0.0027	20.92%	23.84%	68.23%	51.87%
Qilu Lake	Lake Center	0.1432	0.1670	0.1671	0.1616	0.1588	16.59%	16.68%	12.88%	10.89%
	Majiawan	0.1322	0.1573	0.1575	0.1572	0.1581	19.01%	19.11%	18.88%	19.58%
Xingyun Lake	Lkae Center	0.1298	0.1340	0.1345	0.1344	0.1314	3.20%	3.58%	3.56%	1.23%
	Haimen	0.1384	0.1573	0.1535	0.1609	0.1531	13.63%	10.92%	16.29%	10.61%
Yangzong Lake	Lake center	0.0138	0.0137	0.0139	0.0135	0.0134	0.41%	0.88%	2.01%	3.12%
	Tangchi	0.0099	0.0122	0.0123	0.0119	0.0118	23.29%	24.18%	19.97%	18.72%
Yilong Lake	Lake Center	0.1352	0.2251	0.2250	0.2269	0.2231	66.46%	66.41%	67.83%	65.01%
	Dam Center	0.1464	0.2106	0.2094	0.2220	0.2277	43.82%	43.04%	51.65%	55.52%

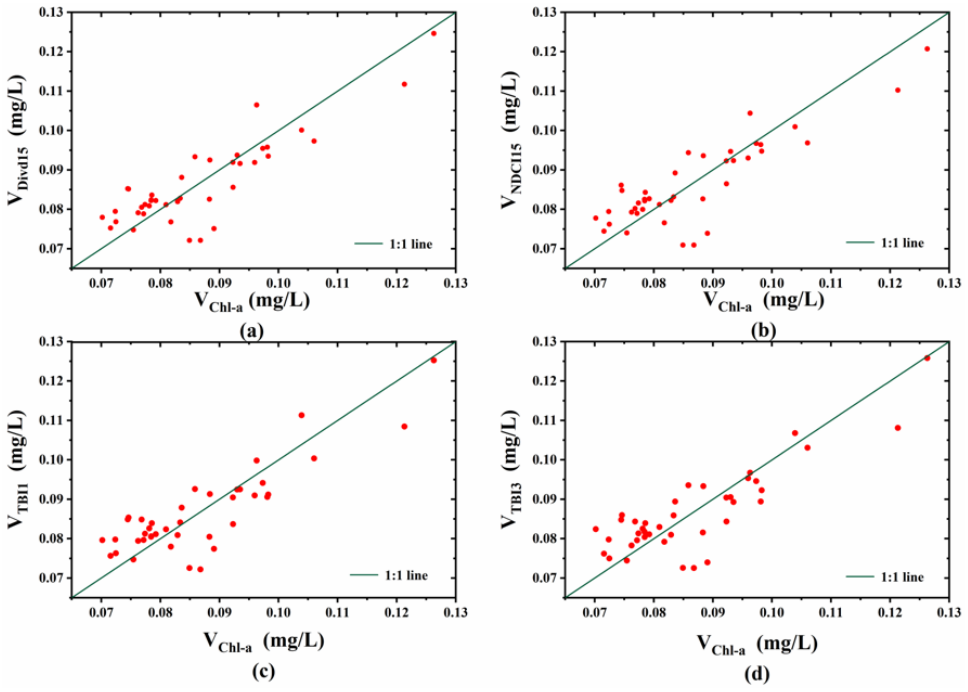

Figure 3. Scatter plot of the retrieved and measured chlorophyll-a concentrations in Dianchi Lake. Subfigures (**a**–**d**) show the 1:1 line between the simulated chlorophyll-a concentration and the measured chlorophyll-a concentration by Divd15, NDCI15, TBI1 and TBI3, respectively.

Table 7. Total accuracy statistics of the CCAPL retrieval model.

Accuracy Assess	Divd15	NDCI15	TBI1	TBI3
RMSE	0.0253	0.0249	0.0265	0.0263
MAE	0.0146	0.0142	0.0150	0.0145
MAPE	26.80%	26.30%	28.21%	27.00%

4.3. Retrieval of the CCAPL

The retrieval model of the CCAPL was selected according to the results of the RF algorithm feature importance, and the accuracy of the model could meet the requirements of the CCAPL retrieval. The CCAPL was retrieved from the Sentinel-2 images of nine plateau lakes in Yunnan Province, and the obtained distribution of the CCAPL is shown in Figure 4.

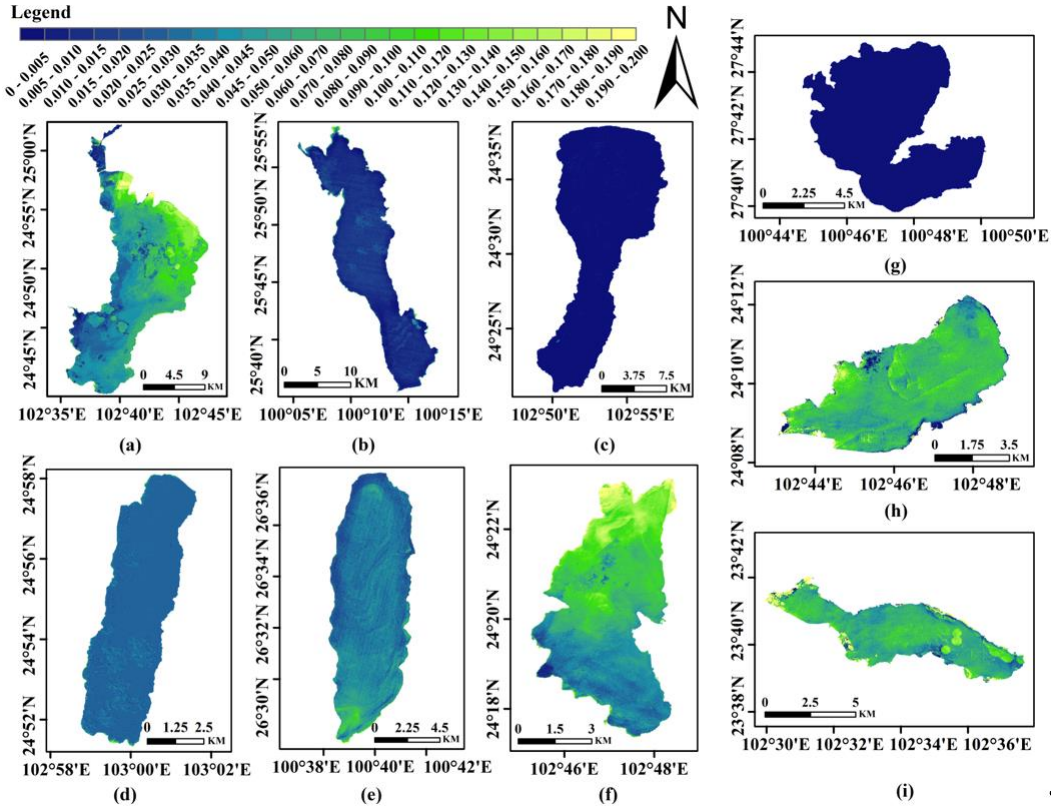

Figure 4. Retrieval of the chlorophyll-a concentrations in nine plateau lakes on 22 and 24 June 2020. (**a**) DCL, (**b**) ERL, (**c**) FXL, (**d**) YZL, (**e**) CHL, (**f**) XYL, (**g**) LGL, (**h**) QLL and (**i**) YLL.

According to the retrieval results of the CCAPL, the green and yellow parts were the regions with high CCAPLs. From the spatial distribution of the CCAPL, the chlorophyll-a concentrations in Erhai Lake, Fuxian Lake, Lugu Lake and Yangzong Lake were low and evenly distributed, and the chlorophyll-a concentrations in the whole lakes were below 0.02 mg/L, indicating good water quality. The chlorophyll-a concentrations were low in the central and northern parts of Chenghai Lake, but high in the southern part of Chenghai Lake. The chlorophyll-a concentration in the northeastern part of Dianchi Lake was high, while the chlorophyll-a concentrations in the southern and western parts of Dianchi Lake were low, and the mean value of chlorophyll-a concentration in Dianchi Lake was 0.08 mg/L. In the northern part of Xingyun Lake, Qilu Lake and the southeastern part of Yilong Lake, the chlorophyll-a concentrations were high at more than 0.1 mg/L.

4.4. Retrieval of the STPL

Based on the water surface temperature retrieval method, (14) was used for the radiative transfer process and the Landsat-8 TIRS sensor Band 10 was used to invert the lake surface temperature through the single-channel method. The radiation brightness was obtained via radiative calibration. The land surface emissivity was determined based on the normalized difference vegetation index (NDVI) threshold classification.

The vegetation coverage was calculated using (16), and then the land surface emissivity was calculated using (15). The atmospheric upward radiation, atmospheric downward radiation and atmospheric transmittance were derived by simulating the radiation transport from the ground to the atmosphere using ACPC input parameters on the NASA website. The atmospheric transmittance of the nine plateau lakes simulated using ACPC was 0.55, the atmospheric upward radiation was 3.32 and the atmospheric downward radiation was 5.10. The water surface temperature was calculated using (17), and the retrieval results are shown in Figure 5.

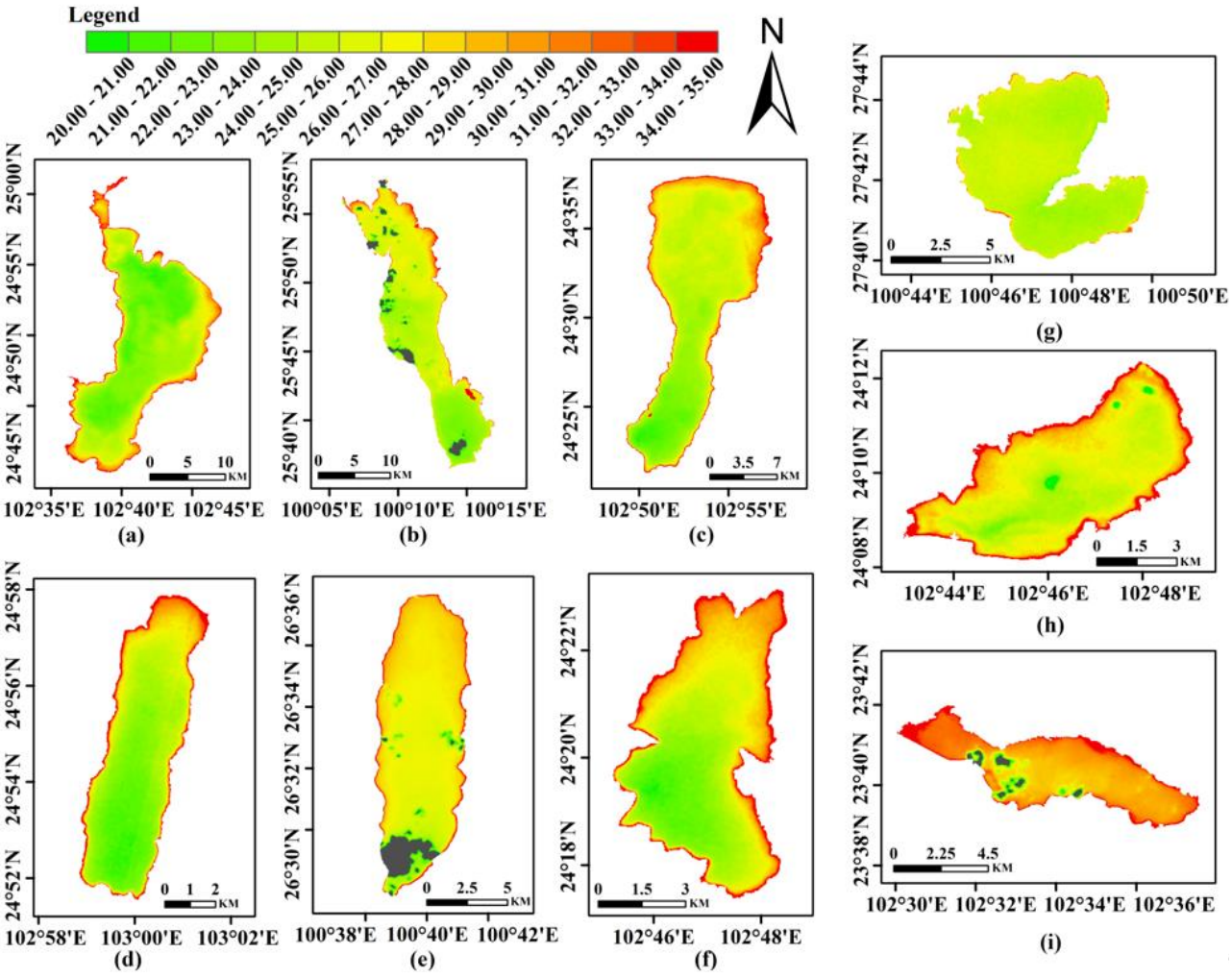

Figure 5. Retrieval of the water surface temperatures in nine plateau lakes on 22 and 24 June 2020. (**a**) DCL, (**b**) ERL, (**c**) FXL, (**d**) YZL, (**e**) CHL, (**f**) XYL, (**g**) LGL, (**h**) QLL and (**i**) YLL.

In Figure 5, the gray part represents the cloud, and the data was missing. The green part represents the low surface temperature of the lakes. The red parts represent high lake surface temperatures. Because the study was undertaken in summer, the surface temperatures of the nine plateau lakes were above 20 degrees Celsius, among which the average temperature of Yilong Lake was 31.86 °C and Lugu Lake was 22.41 °C. From the perspective of the distribution of temperature, the temperatures of the lakes near the shore

area rose obviously and the temperature decreased in the lakes area. This was because the lakes had a strong heat capacity, a water supply, and a large area, causing the average temperatures near the lakes to remain significantly lower; this result in meteorology is often referred to as the "lake effect" [35]. To sum up, the lake temperature retrieval basically met the requirements.

4.5. Spatial Correlation Analysis

Based on the CCAPL and STPL retrieval results, the lake temperatures and corresponding chlorophyll-a contents were extracted. The relationship between the lake temperature and chlorophyll-a content is shown in Figure 6. When the chlorophyll-a content was very low, there was no correlation between them; when the content of chlorophyll-a was larger than 0.05 mg/L, with the increase in temperature, chlorophyll-a had a good linear correlation with lake temperature.

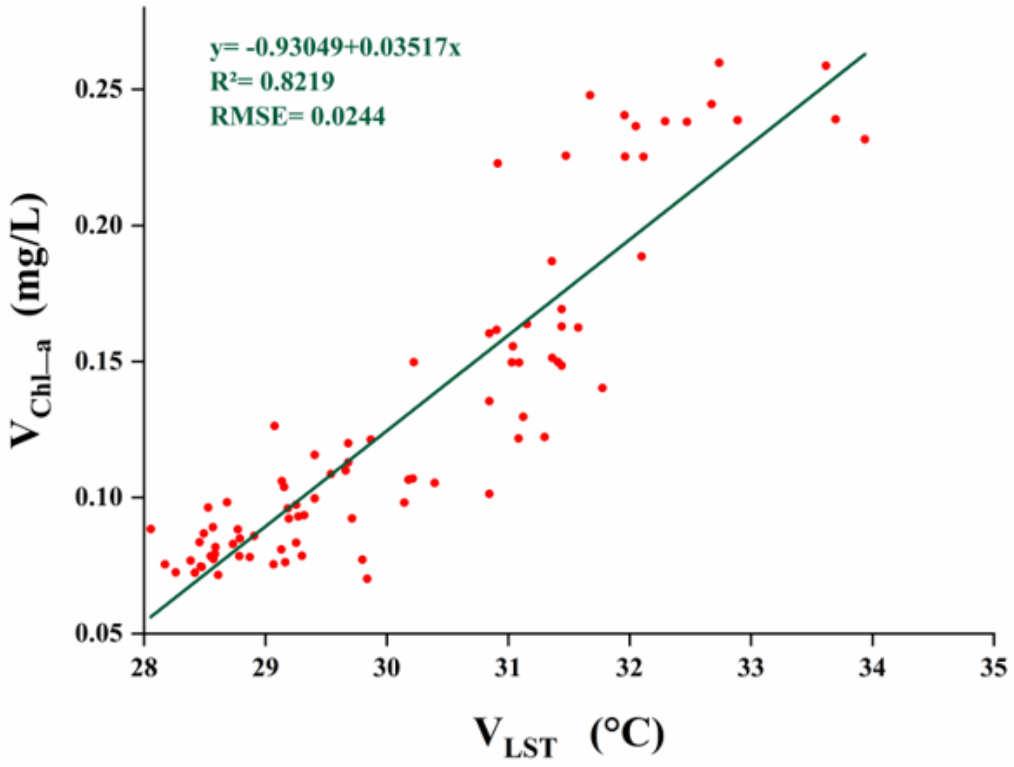

Figure 6. Linear correlation between the CCAPL and the STPL.

In addition, the spatial superposition analysis was carried out on nine plateau lakes, and the temperatures and chlorophyll-a concentrations were taken as the influencing factors, with weights of 0.4 and 0.6, respectively. The resulting images are shown in Figure 7. These images show the regions associated with the STPL and CCAPL, where the dark yellow regions show the highest increase in chlorophyll-a concentration at lake temperatures between 20 and 35 °C.

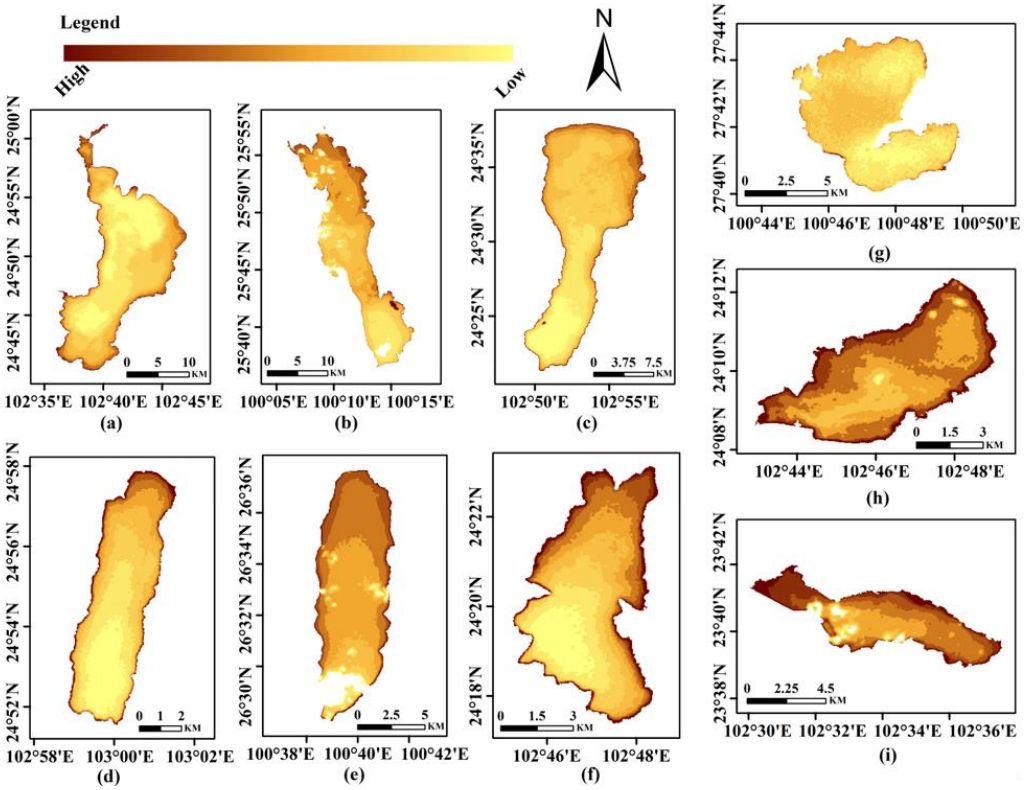

Figure 7. Retrieval of the water surface temperature in nine plateau lakes on 22 and 24 June 2020. (**a**) DCL, (**b**) ERL, (**c**) FXL, (**d**) YZL, (**e**) CHL, (**f**) XYL, (**g**) LGL, (**h**) QLL and (**i**) YLL.

5. Discussion

First, from the abovementioned experimental results, it can be seen that the Sentinel-2 red-edge bands produced good results regarding the CCAPL retrieval. However, due to the plateau lakes' chlorophyll-a-concentration-monitoring satellites having low temporal and spectral resolutions, it is difficult for the measurements of the multi-spectral satellites to satisfy the monitoring of chlorophyll-a in plateau lakes. Considering that hyperspectral satellites will be launched later, the monitoring capability is expected to be improved through multi-satellite networking in the future. Second, the Landsat-8 TIRS single-channel algorithm based on the retrieval of land surface temperature achieved good results. However, due to the large deviation of the Landsat-8 Band 11 calibration, the USGS does not encourage the use of dual-channel temperature retrieval. With the advent of Landsat-9, in the future, a dual-channel algorithm based on Landsat-9 TIRS data can be developed for temperature retrieval. Third, although the correlation between the STPL and the CCAPL was verified in this study, the temperature retrieval data selected in this study was from June 2022, which is one of the highest summer temperature months in Yunnan Province. Limited by the time range of the measured chlorophyll-a concentration data and remote sensing satellite imagery data, the results of this study can only be used during the period of the summer temperature rise, which provides little convenience when studying the correlation between the two. We plan to obtain more chlorophyll-a data in future studies and explore the temperature pattern of the plateau lakes in different months, as well as the correlations between temperature and chlorophyll-a in different months. Finally, although the image-based remote sensing reflectance estimation method for the water surface achieved good results, more accurate remote sensing reflectance acquisition can further improve the accuracy of the CCAPL retrieval. Therefore, it is necessary to further develop atmospheric correction methods for remote sensing data, such as the near-infrared dark target method for clean water and the shortwave infrared dark target method for turbid water.

6. Conclusions

In this study, based on in situ measured data and Sentinel-2 satellite reflectance data, we used the feature importance of the RF algorithm screening model and selected four models to conduct the retrieval experiment for the CCAPL. The applicability and retrieval accuracy of the four models in the Sentinel-2 images were analyzed. In addition, the Landsat-8 TIRS single-channel algorithm was used for the STPL retrieval of the plateau lakes, and the correlation between the STPL and the CCAPL was also analyzed. The main conclusions were as follows:

(1) According to the ranked RF feature importance, the spectral indexes that strongly correlated with the chlorophyll-a concentration were selected for the CCAPL retrieval. We analyzed the relative error and accuracy. Among the four models, NDCI15 had the best accuracy, with an RMSE of 0.0249, an MAE of 0.0142 and a MAPE of 26.30%.

(2) The lakes with chlorophyll-a concentrations of less than 0.03 mg/L were Chenghai Lake, Yangzong Lake, Erhai Lake, Fuxian Lake and Lugu Lake, among which the chlorophyll-a concentrations of Erhai Lake, Fuxian Lake and Lugu Lake were less than 0.01 mg/L. The lakes with chlorophyll-a concentrations between 0.03 and 0.1 mg/L were Dianchi Lake and Xingyun Lake. The average value of the chlorophyll-a concentration in the northeast of Dianchi Lake and the north of Xingyun Lake was 0.085 mg/L. The lakes with chlorophyll-a concentrations greater than 0.1 mg/L were Yilong Lake and Qilu Lake, among which the chlorophyll-a concentration in Qilu Lake was greater than 0.14 mg/L.

(3) When the STPL was within 28–34 °C, it had an obvious correlation with the chlorophyll-a concentration, and the correlation increased gradually from the lakes' center to the shore. When the lakes' temperatures rise, this provides a key monitoring area for managers. Considering the relatively limited surface monitoring data, the next plan is to accumulate more surface experimental data for the plateau lakes, conduct seasonal analysis or add other hydrological factors to explore the coupling mechanism of the CCAPL and other impurities in the water.

Author Contributions: Conceptualization, D.W. and B.-H.T.; software, D.W., Z.F. and M.L.; validation, B.-H.T. and X.P.; formal analysis, D.W., L.H. and G.C.; data curation, B.-H.T.; writing—original draft preparation, D.W.; writing—review and editing, D.W. and B.-H.T.; funding acquisition, B.-H.T. All authors read and agreed to the published version of the manuscript.

Funding: This research was funded by the Platform Construction Project of High-Level Talent in KUST, and in part by the National Natural Science Foundation of China under grant 41871244, and in part funded by the Regional Science Foundation grant 41961053.

Data Availability Statement: The chlorophyll-a concentration data can be found at http://lake.geodata.cn/ (accessed on 11 November 2021). The Atmospheric Correction Parameter Calculator (ACPC) can be found at https://atmcorr.gsfc.nasa.gov/(accessed on 20 November 2021). The Sentinel-2 MSI surface reflectance data and Landsat-8 TIRS data were provided by the USGS at https://www.usgs.gov/(accessed on 3 December 2021).

Acknowledgments: The authors would like to thank the Yunnan Provincial Department of Ecology and Environment and Nanjing Institute of Geography and Limnology, Chinese Academy of Sciences, for providing the in situ measured chlorophyll-a concentration. We also appreciate the constructive suggestions from reviewers and editors that helped to improve this article.

Conflicts of Interest: The authors declare no conflict of interest.

References

1. Zhang, Y.; Ma, R.; Liang, Q.; Guan, B.; Loiselle, S. Secondary impacts of eutrophication control activities in shallow lakes: Lessons from aquatic macrophyte dynamics in Lake Taihu from 2000 to 2015. *Freshw. Sci.* **2019**, *38*, 802–817. [CrossRef]
2. An, Y.; Kampbell, D. Monitoring Chlorophyll- a as a Measure of Algae in Lake Texoma Marinas. *Bull. Environ. Contam. Toxicol.* **2003**, *70*, 606–611. [CrossRef]

3. Caballero, I.; Navarro, G. Monitoring cyanoHABs and water quality in Laguna Lake (Philippines) with Sentinel-2 satellites during the 2020 Pacific typhoon season. *Sci. Total. Environ.* **2021**, *788*, 147700–147712. [CrossRef]
4. Palmer, S.; Kutser, T.; Hunter, P. Remote sensing of inland waters: Challenges, progress and future directions. *Remote Sens. Environ.* **2014**, *157*, 1–8. [CrossRef]
5. Xu, J.; Gao, C.; Wang, Y. Extraction of spatial and temporal patterns of concentrations of chlorophyll-a and total suspended matter in poyang lake using GF-1 satellite data. *Remote Sens.* **2020**, *12*, 622. [CrossRef]
6. Tilstone, G.; Pardo, S.; Dall'Olmo, G.; Brewin, R.; Nencioli, F.; Dessailly, D.; Kwiatkowska, E.; Casal, T.; Donlon, C. Performance of Ocean Colour Chlorophyll a algorithms for Sentinel-3 OLCI, MODIS-Aqua and Suomi-VIIRS in open-ocean waters of the Atlantic. *Remote Sens. Environ.* **2021**, *260*, 112444. [CrossRef]
7. Mark, A.; Stefan, G.; Nick, S. Complementary water quality observations from high and medium resolution Sentinel sensors by aligning chlorophyll-a and turbidity algorithms. *Remote Sens. Environ.* **2021**, *265*, 112651.
8. Pahlevan, N.; Smith, B.; Binding, C.; Gurlin, D.; Li, L.; Bresciani, M.; Giardino, C. Hyperspectral retrievals of phytoplankton absorption and chlorophyll-a in inland and nearshore coastal waters. *Remote Sens. Environ.* **2021**, *253*, 112200. [CrossRef]
9. Wu, H.; Liao, M.; Guo, J.; Zhang, Y.; Liu, Q.; Li, Y. Diatom assemblage responses to multiple environmental stressors in a deep brackish plateau lake, SW China. *Environ. Sci. Pollut. Res. Int.* **2022**, *29*, 33117–33129. [CrossRef] [PubMed]
10. Luo, J.; Qin, L.; Mao, P.; Xiong, Y.; Zhao, W.; Gao, H.; Qiu, G. Research Progress in the Retrieval Algorithms for Chlorophyll-a, a Key Element of Water Quality Monitoring by Remote Sensing. *Int. Remote Sens.* **2021**, *36*, 473–488.
11. Sagan, V.; Peterson, K.; Maimaitijiang, M.; Sidike, P.; Sloan, J.; Greeling, B.; Maalouf, S.; Adamset, C. Monitoring inland water quality using remote sensing: Potential and limitations of spectral indices, bio-optical simulations, machine learning, and cloud computing. *Earth-Sci. Rev.* **2020**, *205*, 103187. [CrossRef]
12. Liu, C.; Zhu, L.; Li, J.; Wang, J.; Ju, J.; Qiao, B.; Ma, Q.; Wang, S. The increasing water clarity of Tibetan lakes over last 20 years according to MODIS data. *Remote Sens. Environ.* **2021**, *253*, 112199. [CrossRef]
13. Seegers, B.; Werdell, P.; Vandermeulen, R.; Salls, W.; Stumpf, R.; Schaeffer, B.; Owens, T.; Bailey, S.; Scott, J.; Loftin, K. Satellites for long-term monitoring of inland U.S. lakes: The MERIS time series and application for chlorophyll-a. *Remote Sens. Environ.* **2021**, *266*, 112685. [CrossRef]
14. Xu, Y.; Dong, X.; Wang, J. Use of Remote Multispectral Imaging to Monitor Chlorophyll-a in Taihu Lake: A Comparison of Four Machine Learning Model. *J. Hydroecol* **2019**, *40*, 48–57.
15. Zhang, Q.; Wu, Z. Research progress of the inversion algorithm of chlorophyll-a concentration in estuaries and coastal waters. *Ecol. Sci.* **2017**, *36*, 215–222.
16. Wang, H.; Yang, F.; Luo, Z. An experimental study of the intrinsic stability of random forest variable importance measures. *BMC Bioinform.* **2016**, *17*, 60–78. [CrossRef] [PubMed]
17. Wu, Z.; Li, J.; Wang, R.; Shi, L.; Miao, S.; Lv, H.; Li, Y. Estimation of CDOM concentration in inland lake based on random forest using Sentinel-3A OLCI. *J. Environ. Sci.* **2018**, *30*, 979–991.
18. Hang, X.; Li, Y.; Li, X.; Xu, M.; Sun, L. Estimation of Chlorophyll-a Concentration in Lake Taihu from Gaofen-1 Wide-Field-of-View Data through a Machine Learning Trained Algorithm. *J. Meteorol. Res.* **2022**, *36*, 208–226. [CrossRef]
19. Xu, H. Retrieval of the reflectance and land surface temperature of the newly-launched Landsat 8 satellite. *Chinese J. Geophys.* **2015**, *58*, 741–747.
20. Duan, S.; Ru, C.; Li, Z.; Wang, M.; Xu, H.; Li, H.; Wu, P.; Zhan, W.; Zhou, J.; Zhao, W.; et al. Reviews of methods for land surface temperature retrieval from Landsat thermal infrared data. *Natl. Remote Sens. Bull.* **2021**, *25*, 1591–1617.
21. Holm-Hansen, O.; Lorenzen, C.; Holmes, R.; Strickland, J. Fluorometric Determination of Chlorophyll. *J. Cons. Int. Explor. Mer.* **1965**, *30*, 3–15. [CrossRef]
22. Rahmat, A.; Daruati, D.; Ramadhani, W.; Ratnawati, H. Analysis of Normalized Different Wetness Index (NDWI) Using Landsat Imagery in the Ciletuh Geopark Area as Ecosystem Monitoring. *IOP Conf. Ser. Earth Environ. Sci.* **2022**, *1062*, 012037. [CrossRef]
23. Xu, H. A Study on Information Extraction of Water Body with the Modified Normalized Difference Water Index (MNDWI). *J. Remote Sens.* **2005**, *09*, 589–595.
24. Gordon, H.R.; Morel, A. *Remote Assessment of Ocean Color for Interpretation of Satellite Visible Imagery: A Review*; Springer: New York, NY, USA, 1983; Volume 37, p. 292.
25. Liu, X.; Steele, C.; Simis, S.; Warren, M.; Tyler, A.; Spyrakos, E.; Selmes, N.; Hunter, P. Retrieval of Chlorophyll-a concentration and associated product uncertainty in optically diverse lakes and reservoirs. *Remote Sens. Environ.* **2021**, *267*, 112710. [CrossRef]
26. Dekker, A.; Peters, S. The Use of the Thematic Mapper for the Analysis of Eutrophic Lakes: A Case Study in The Netherlands. *Int. J. Remote Sens.* **1993**, *14*, 799–822. [CrossRef]
27. Lu, L.; Gong, Z.; Liang, Y.; Liang, S. Retrieval of Chlorophyll-a Concentrations of Class II Water Bodies of Inland Lakes and Reservoirs Based on ZY1-02D Satellite Hyperspectral Data. *Remote Sens.* **2022**, *14*, 1842. [CrossRef]
28. Shi, H.; Li, X.; Niu, Z.; Li, J.; Li, Y.; Li, N. Remote sensing information extraction of aquatic vegetation in Lake Taihu based on Random Forest Model. *J. Lake Sci.* **2016**, *28*, 635–644.
29. Ananias, P.; Negri, R.; Dias, M.; Silva, E.; Casaca, W. A Fully Unsupervised Machine Learning Framework for Algal Bloom Forecasting in Inland Waters Using MODIS Time Series and Climatic Products. *Remote Sens.* **2022**, *14*, 4283. [CrossRef]
30. Goldstein, B.; Polley, E.; Briggs, F. Random Forests for Genetic Association Studies. *Stat. Appl. Genet. Mol. Biol.* **2011**, *10*, 32. [CrossRef]

31. Minnett, P. Radiometric measurements of the sea-surface skin temperature: The competing roles of the diurnal thermocline and the cool skin. *Int. J. Remote Sens.* **2003**, *24*, 5033–5047. [CrossRef]
32. Pyle, J. Planck's radiation law: Spectral distribution and the gamma functions. *J. Chem. Educ.* **1985**, *62*, 488. [CrossRef]
33. Qin, Z.; Li, W.; Xu, B.; Zhang, W. Estimation method of land surface emissivity for retrieving land surface temperature from Landsat TM6 data. *Adv. Mar. Sci.* **2004**, *22*, 129–137.
34. Duan, S.; Li, Z.; Wang, C.; Zhang, S.; Tang, B.; Leng, P.; Gao, M. Land-surface temperature retrieval from Landsat 8 single-channel thermal infrared data in combination with NCEP reanalysis data and ASTER GED product. *Int. J. Remote Sens.* **2019**, *40*, 1763–1778. [CrossRef]
35. Burnett, A.; Kirby, M.; Mullins, H.; Patterson, W. Increasing Great Lake-Effect Snowfall during the Twentieth Century: A Regional Response to Global Warming? *J. Clim.* **2003**, *16*, 3535–3542. [CrossRef]